Supporting Information

The key role of soft corona into the superlattice formation of CeO_2 nanoparticles

Noemi Gallucci[1,2], Alessandro Cangiano[1,2], Rosario Oliva[1], Donato Ciccarelli[1,2], Gennaro Rollo[3], Rocco Di Girolamo[1], Nathan Cowieson[4], Giuseppe Vitiello[2,5], Luigi Paduano[1,2,]*

[1]Department of Chemical Sciences, University of Naples Federico II, 80126, Naples, Italy

[2]CSGI, Center for Colloid and Surface Science, 50019, Sesto Fiorentino, Italy

[3]CNR-IPCB Istituto per i Polimeri, Compositi e Biomateriali, 80055, Portici, Italy

[4]Diamond Light Source, Didcot, Oxfordshire, England, United Kingdom

[5]Department of Chemical, Materials and Production Engineering, University of Naples Federico II, 80125, Naples, Italy

Synthesis conditions

Table S1. Synthesis conditions: capping agent, acronym, volume, and synthesis temperatures.

Capping Agent	Acronym	Volume ± 0.01 mL	150 °C	200 °C	250 °C
octylamine	C8	1.98	X		
decylamine	C10	2.40	X	X	
dodecylamine	C12	2.77	X	X	
hexadecylamine	C16	3.10	X	X	X
oleylamine	C18	3.95	X	X	X

***Amine@CeO₂ NPs*: investigating the synthesized NPs**

The shape and size of *amine@CeO_2 NPs* are important features for the formation of superlattices. From an overall observation, though TEM images, of different CeO_2 NPs synthesized at three different temperatures and considering amines with different lengths of the alkyl chains as capping agents, shape, size, and tendency to self-assembly strongly depend on these synthesis conditions. In fact, as the length of the alkyl chain and the synthesis temperature increase, the size of CeO_2 NPs decreases as well as the tendency of the self-assembly, as shown in Figure S1.

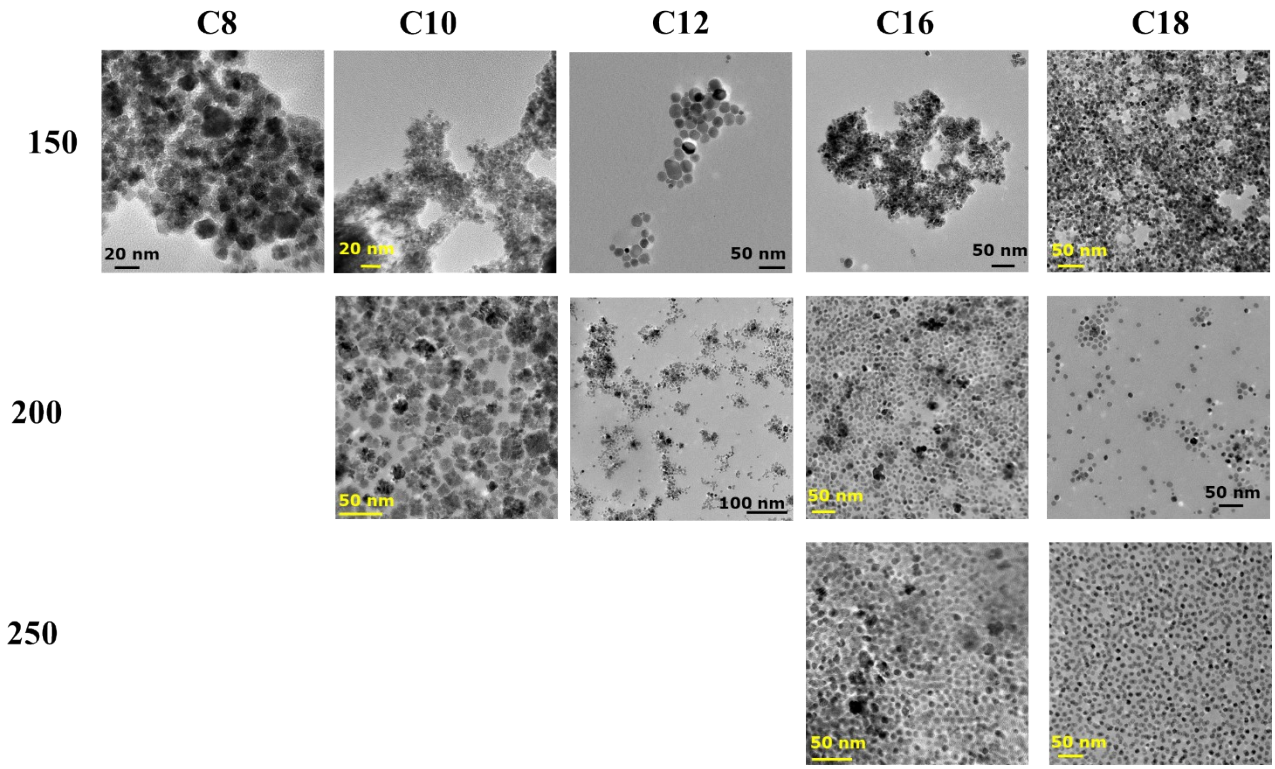

Figure S1. TEM images of *amine@CeO_2 NPs* (scale bar: 20, 50, and 100 nm).

Amine@CeO_2 NPs synthesized at 150 and 200 °C exhibit irregular morphology and a strong tendency to self-assembly, only *C18@CeO_2* synthesized at 200 °C has a spherical shape and a less tendency to self-assembly. From the TEM images, it is evident that the NPs synthesized at 250 °C are smaller than the others, and that *C18@CeO_2 NPs* are spherical and monodispersed. However, by assimilating all synthesized NPs to spheres it is possible, by a statistical analysis, to determine the mean radius of the inorganic core <R>. The results obtained were reported in Figure S2. The *C10@CeO_2* synthesized at 150 °C has a larger average size (~10 nm) than the others. <R>

decreases in the case of synthesis with C8 (~ 6.4 nm), and then becomes constant and equal to about 4 nm for the other NPs synthesized at 150 °C (Figure S2A). All *amine@CeO₂* synthesized at 200 °C have an average size between 3 and 4 nm (Figure S2B). Instead, the mean radii of the inorganic core of *amine@CeO₂* synthesized at 250 °C are smaller than all other samples, in fact, they turn out to be 2.9 and 2.5 for *C16@CeO₂* and *C18@CeO₂*, respectively. These results indicate that a moderate synthesis temperature (150 or 200 °C) could be sufficient to allow NPs with a mean radius equal to or less than 10 nm, although with an irregular shape, to be obtained. However, only the longest amine and the highest temperature allow to obtain spherical and monodisperse NPs.

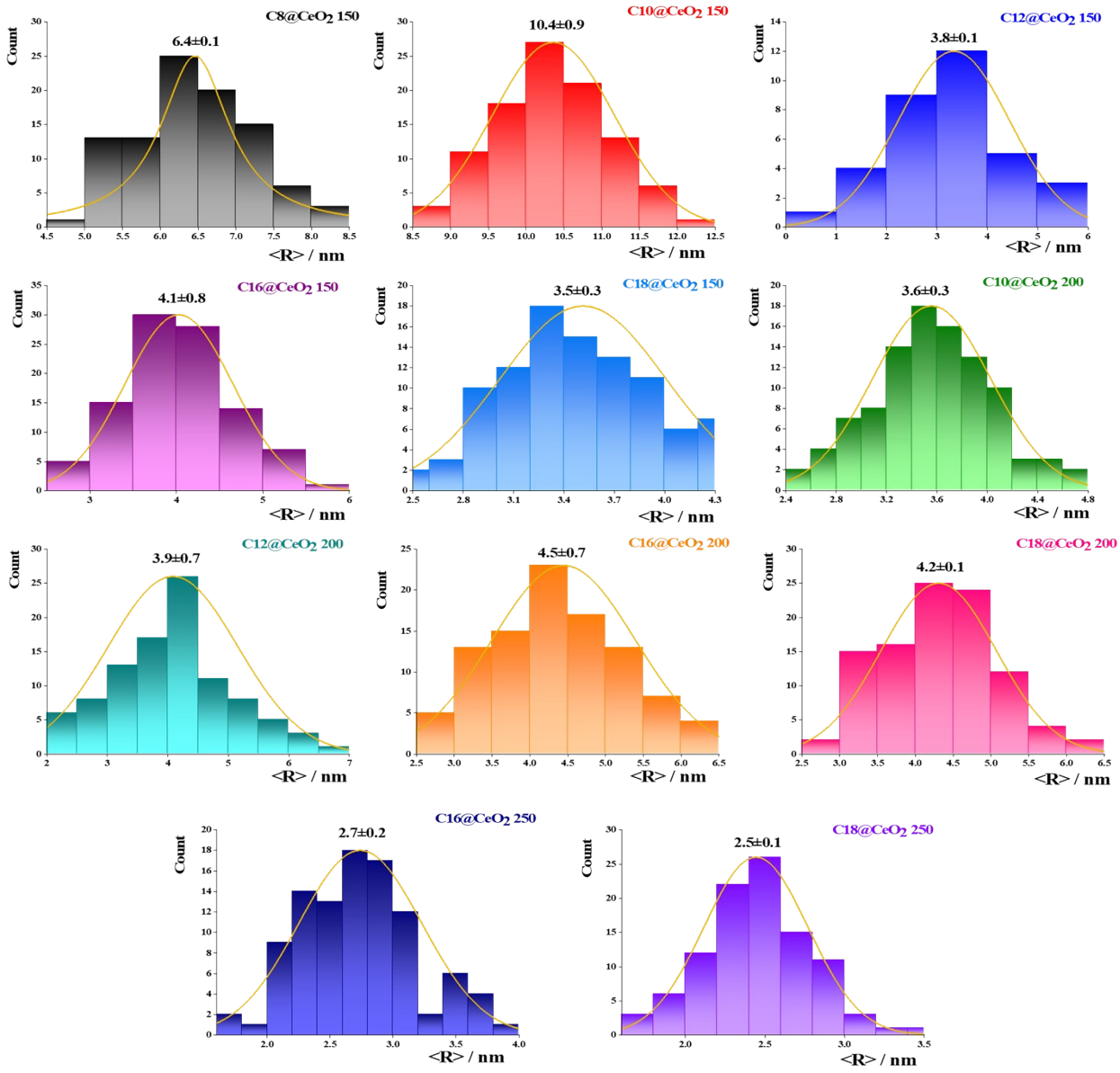

Figure S2. Size distribution histograms of *amine@CeO₂ NPs*.

To verify whether the tendency to aggregate was an artifact of the preparation of the TEM samples, which provide for the evaporation of the solvent, DLS measurements have been carried out (Figure S3). The hydrodynamic radius distributions confirm the tendency to self-assembly also in suspension for all amine@CeO_2 synthesized at 150 °C (Figure S3A, and B), however, the size of the aggregates decreases further with the increase of the synthesis temperature, as shown by the hydrodynamic radius distribution in Figure S3C. This is evident for all NPs synthesized with the same capping agent, but the strongest effect is observed in the case of *C10@CeO_2*, with a R_h of about 920 and 51 nm for synthesis at 150 and 200 °C, respectively. For the *amine@CeO_2* synthesized at 250 °C (Figure S3E), the R_h shows that the *C16@CeO_2* system still tends to self-assembly, while sample *C18@CeO_2* is monodispersed in suspension. Furthermore, considering the R_h value and the core dimension as determined by TEM, a thickness of the coating layer of about 2.5 nm was calculated, in agreement with the C18 length in its full-length extension (2.4 nm). [1–3]

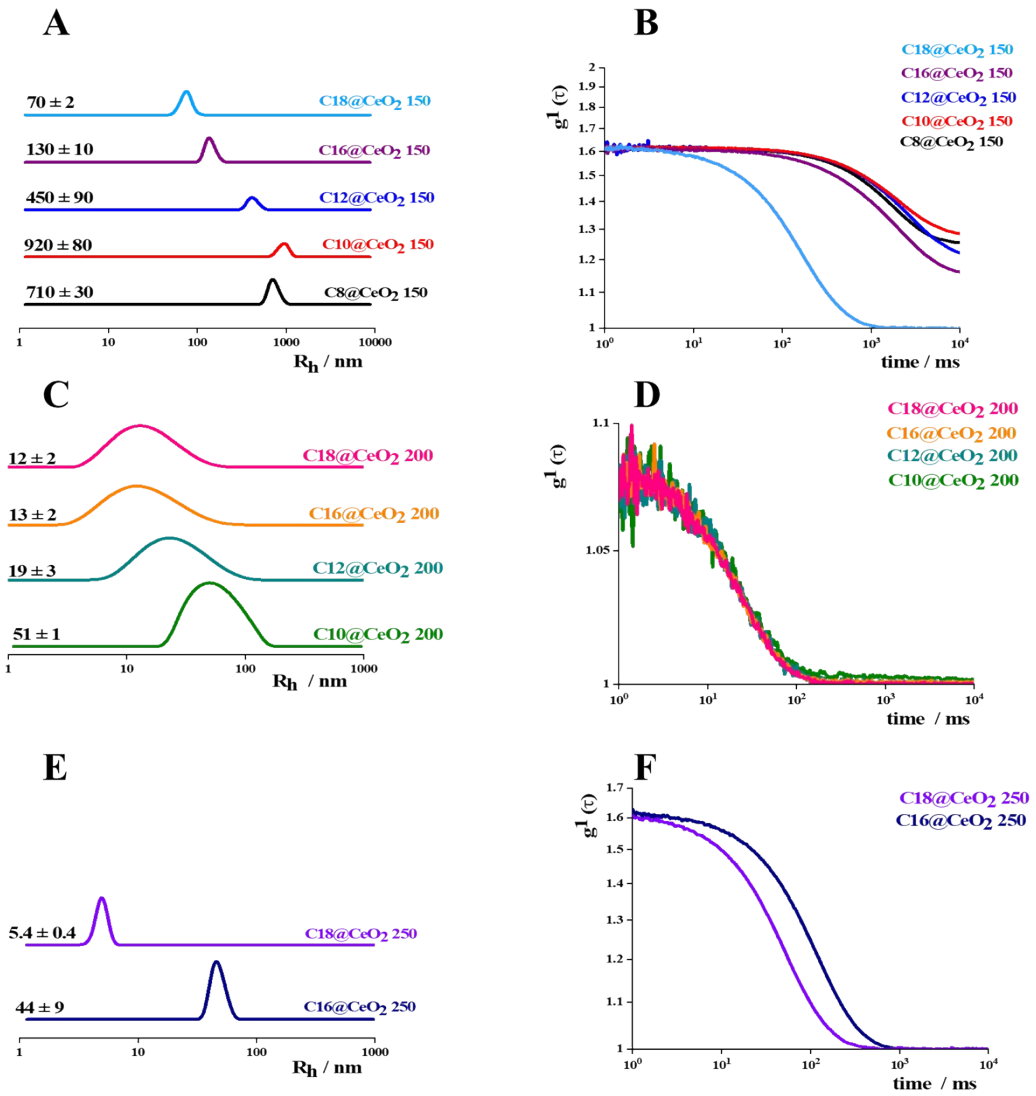

Figure S3. Hydrodynamic radius R_h of *amine@CeO₂ NPs* synthesized at 150 °C **(A)**, 200 °C **(C)**, and 250 °C **(E)** in chloroform, and the corresponding autocorrelation functions **(B, D,** and **F)**.

To confirm the presence of the organic coating on the NP surface, IR spectroscopy measurements were performed (Figure S4). The measurements were carried out in a 4000-400 cm^{-1} range, where the peaks of both the organic coating and CeO_2 should be visible. Indeed, the characteristic peak of CeO_2 falls at about 460 cm^{-1},[4] with a second peak at about 770 cm^{-1}.[5] For all systems are visible both the peaks of the organic and inorganic parts. The bands at 460 and 720 cm^{-1} corresponding to cerium oxide are observed. The wavenumber shift could be due to the presence of the organic coating. Intense bands in the 2800-3000 cm^{-1} region, due to CH stretching, and 1460-1500 cm^{-1} region, due to CH_2 bending confirm a significant presence of the organic coating. It is noteworthy

that all the amines used, except C18 are saturated. Therefore, the presence in all the spectra of the peaks corresponding to CH_2 bending could indicate the capacity of CeO_2 to induce unsaturation.

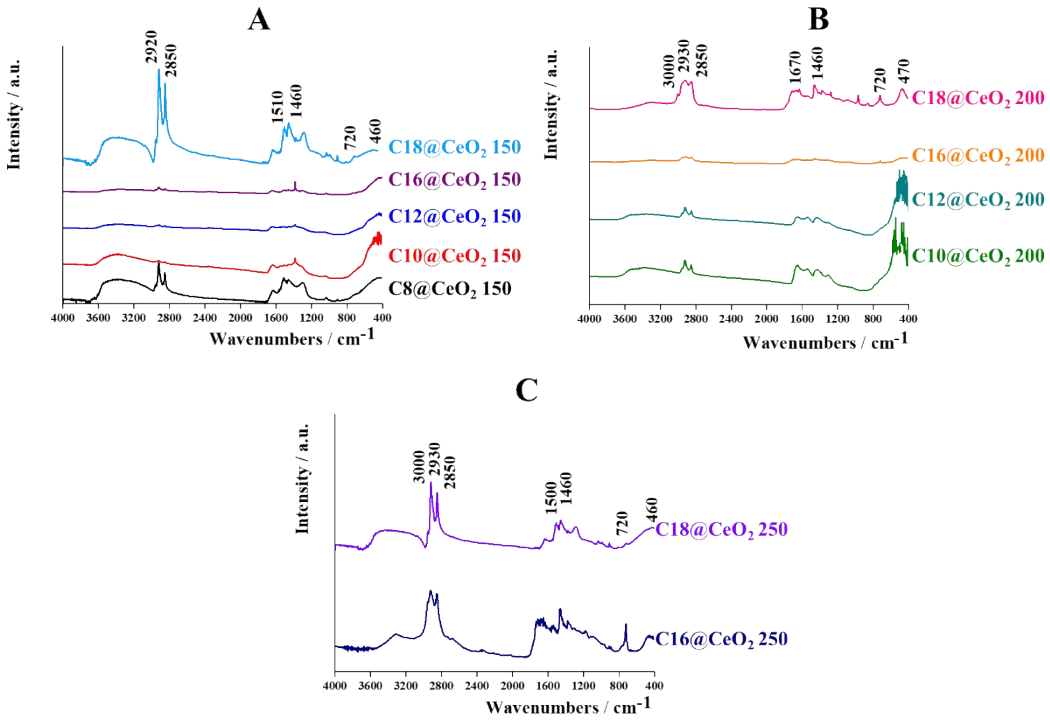

Figure S4. IR spectra of *amine@CeO_2 NPs* synthesized at 150 °C **(A)**, 200 °C **(B)**, and 250 °C **(C)**.

Although with IR was determined qualitatively the presence of the organic coating on the inorganic surface of the nanoparticles, through TGA measurements, it was possible to quantify this presence for the different systems synthesized at 200 °C and 250 °C (Figure S5). The first inflection at about 150 °C, in the TGA curves, could be due to the presence of solvent, while the second inflection is due to material loss as a result of degradation of the organic coating.[6,7] The observed increase in the degradation temperatures of adsorbed amines compared to pure ones is attributed to the fact that adsorbed amines are protected from degradation due to their close proximity to the nanoparticles.[8] From these data, it was possible to calculate the amine density,[9] which turns out to be 1.73 ± 0.06, 2.09 ± 0.14, 5.2 ± 0.1, 4.5 ± 0.2, 3.5 ± 0.2, and 4.6 ± 0.2 chains per nm^2 for *C10@CeO_2 200*, *C12@CeO_2 200*, *C16@CeO_2 200*, *C18@CeO_2 200*, *C16@CeO_2 250*, and *C18@CeO_2 250*,

respectively. These values indicate a partial coating in the case of the first two systems, while a complete coating can be had in the presence of hexadecylamine and oleylamine.[7]

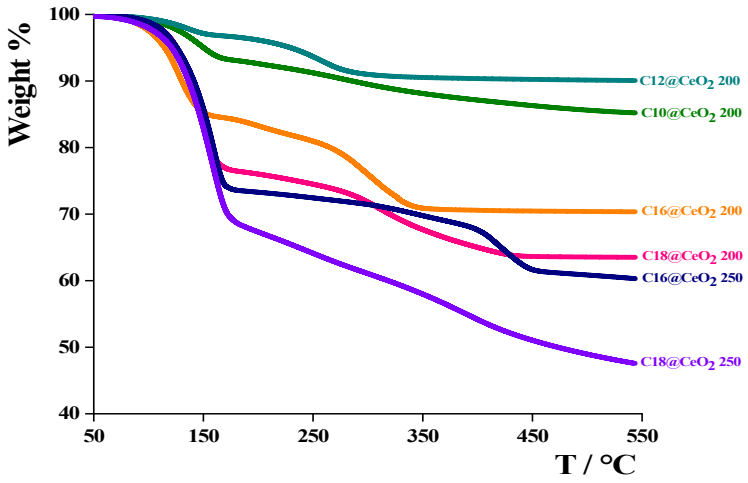

Figure S5. TGA curve of *amine@CeO_2 NPs* synthesized at 200 °C, and 250 °C.

Finally, to assess whether crystalline NPs were synthesized, XRD measurements were performed (Figure S6). The patterns show the typical peaks of a face-centered cubic structure, typical of cerium oxide crystal. The broad halo at 2θ values of less than 28° could be due to the presence of the organic coating on the inorganic core.[1]

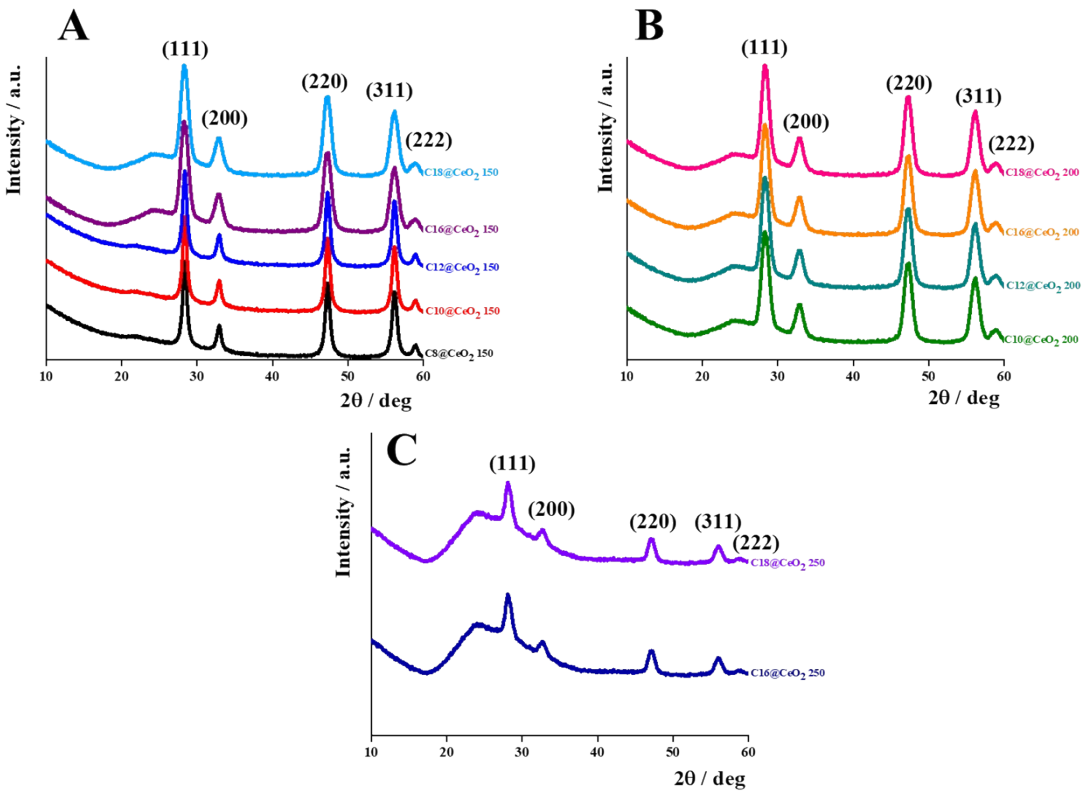

Figure S6. XRD spectra of *amine@CeO_2 NPs* synthesized at 150 °C **(A)**, 200 °C **(B)**, and 250 °C **(C)**.

OA-amine@CeO_2 NPs: superlattices characterization

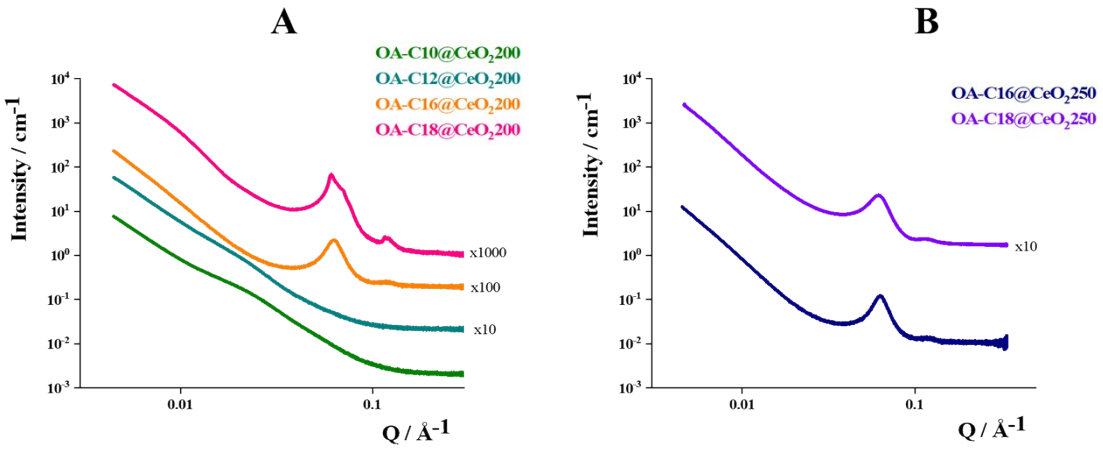

Figure S7. SAXS patterns of *OA-amine@CeO_2 NPs* synthesized at 200 °C **(A)**, and at 250 °C **(B)** in H_2O.

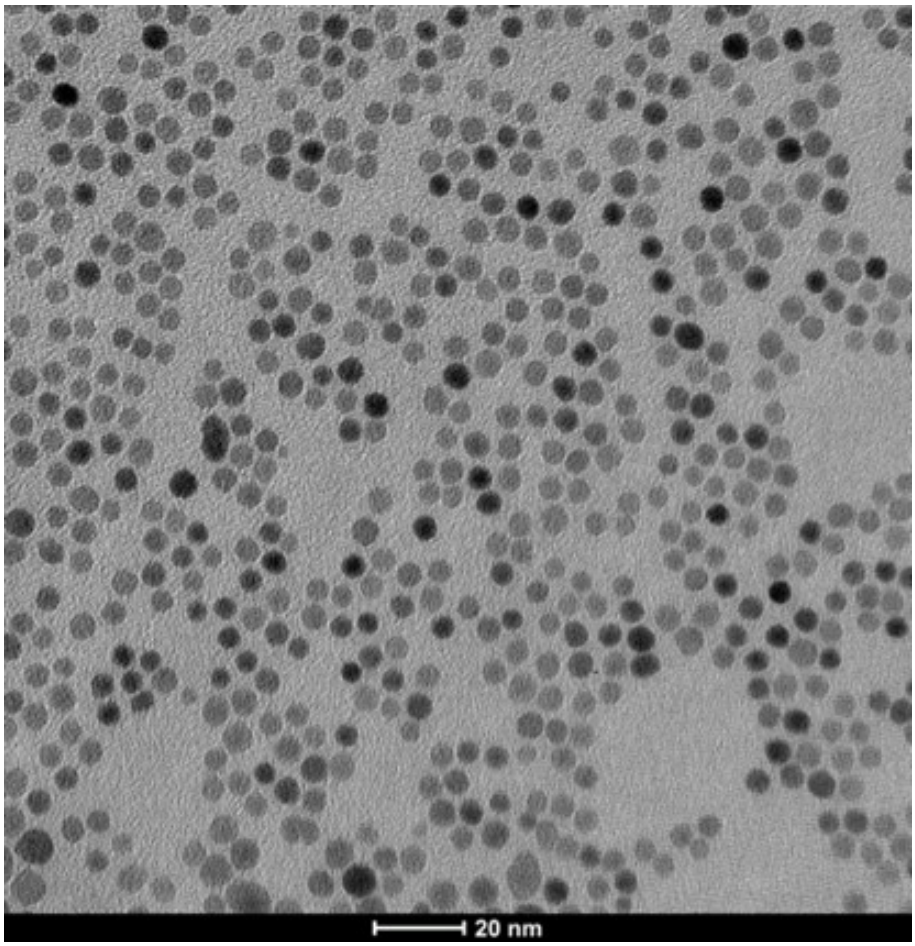

Figure S8. TEM image of *OA-C16@CeO₂ 250* (scale bar: 20 nm).

Table S2. Comparison between the experimental values of *OA-C16@CeO₂ 200* and *OA-C18@CeO₂ 200* samples obtained from SAXS analysis and the theoretical values of FCC and C14 FK structures.[10]

OA-C16@CeO₂ 200		***OA-C18@CeO₂ 200***		**FCC**		**C14 FK**	
Q Å^{-1}	**Q/Q$_1$**	**Q Å^{-1}**	**Q/Q$_1$**	**Q/Q$_1$**	**hkl**	**Q/Q$_1$**	**hkl**
0.06	1	0.06	1	1	111	1	100
		0.07	1.17	1.15	200	1.14	101
0.12	2	0.12	2	2	222	2	200
		0.20	3.33	3.26	440	3.32	205

Table S3. Comparison between the experimental values of *OA-C16@CeO₂ 250* sample obtained from SAXS analysis and the theoretical values of phase C14 FK.[10]

OA-C16@CeO₂ 250		**C14 FK**	
Q Å^{-1}	**Q/Q$_1$**	**Q/Q**	**hkl**

		1	
0.06	1	1	100
0.12	2	2	200

Table S4. Comparison between the experimental values of *OA-C18@CeO₂ 250* sample obtained from SAXS analysis and the theoretical values of phase C14 FK.[2,10]

OA-C18@CeO₂ 250		**C14 FK**	
Q Å^{-1}	**Q/Q₁**	**Q/Q₁**	**hkl**
0.062	1	1	100
0.118	1.892	1.879	103
0.204	3.286	3.321	205

Table S5. Comparison between the distance obtained from SAXS d_{SAXS} (calculated considering the Q position of the first peak) and microscopy image d_{TEM} (calculated from a statistical analysis of the image).

Sample	d_{SAXS}	d_{TEM}
OA-C10@CeO₂ 200		6
OA-C12@CeO₂ 200	7.8	7
OA-C16@CeO₂ 200	10	7.2
OA-C18@CeO₂ 200	10	7.9
OA-C16@CeO₂ 250	10	7.5
OA-C18@CeO₂ 250	10	7.4

***OA-amine@CeO₂ NPs*: interaction potentials**

Elastic interactions:

$$V_{elas}(d) = \frac{2\pi rkTL^2\rho}{MW}\phi f\left(d - 2rL\right) \qquad \text{(S1)}$$

where k is the Boltzmann constant, T is the temperature, ρ is the ligand density, MW is the molecular weight, ϕ is the fraction of surface coverage by the ligand, d is the distance between two NPs, r is the core radius, and L is the length of the alkyl chains of the ligand.

Osmotic interactions:

$$V_{osm}(d) = \frac{4\pi rkT}{v_1}\phi^2\left(\frac{1}{2} - \chi\right)L^2\left(\frac{d - 2r}{2L} - \frac{1}{4} - ln\left(\frac{d - 2r}{L}\right)\right) \quad \text{(S2)}$$

where k is the Boltzmann constant, T is the temperature, v_1 is the ligand molecular volume, ϕ is the fraction of surface coverage by the ligand, χ is the Flory-Huggin's parameter, d is the distance between two NPs, r is the core radius, and L is the length of the alkyl chains of the ligand.

Hydrophobic interactions:

$$V_{hydro} = -4\pi rD_0\gamma(1 - f)exp\left(-\frac{d - 2r - 2L}{D_0}\right) \quad \text{(S3)}$$

where D_0 is the hydrophobic decay length, γ is the surface tension of the ligand in water, f is a dimensionless parameter that reflects the hydrophobic-hydrophilic balance (set to 0.95), d is the distance between two NPs, r is the core radius, and L is the length of the alkyl chain of the ligand.

Van der Waals interactions:

$$V_{vdW}(d) = -\frac{A}{6}\left[\frac{2r^2}{d^2 - 4r^2} + \frac{2r^2}{d^2} + ln\left(\frac{d^2 - 4r^2}{d^2}\right)\right] \quad \text{(S4)}$$

where d is the center-center distance between two NPs, A is the Hamaker constant (it depends on the interaction between the organic layer on the NP surface and the solvent), and r is the core radius.

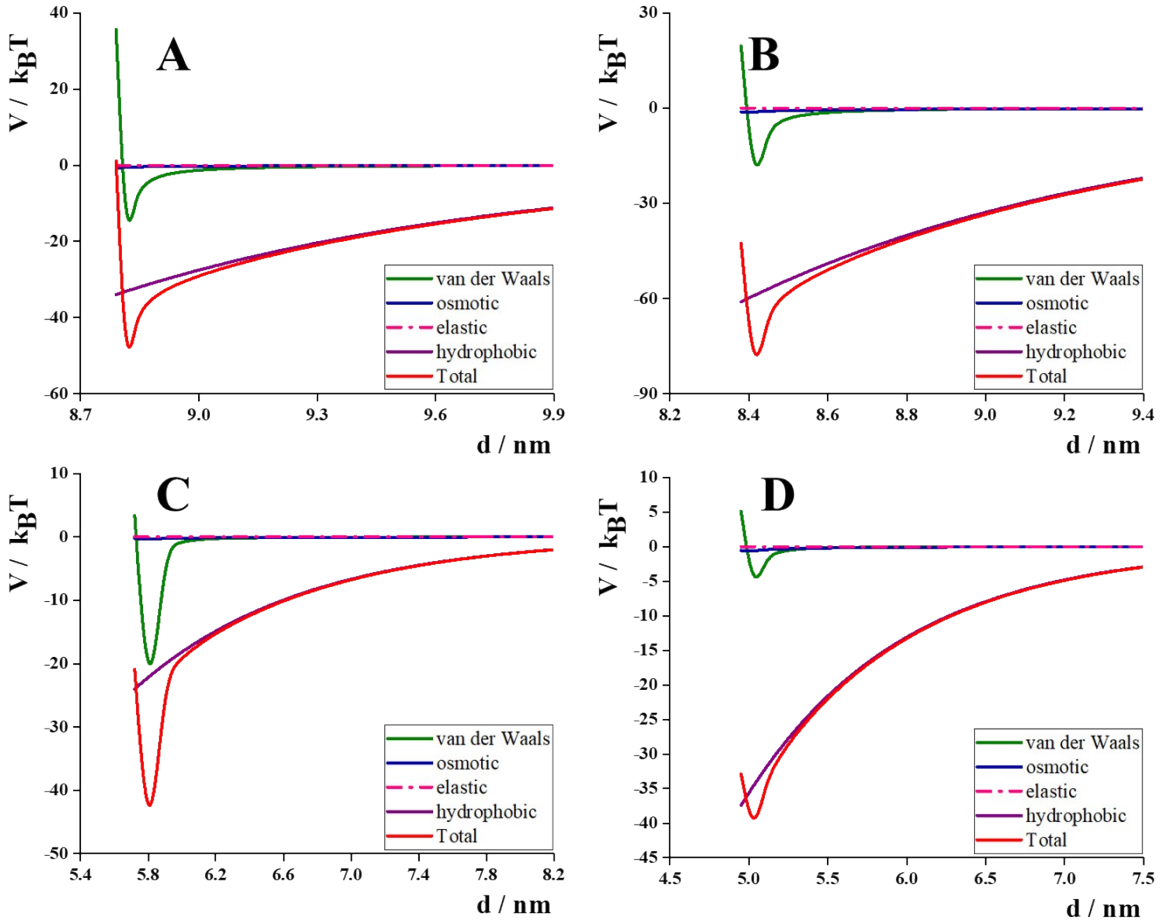

Figure S9. van der Waal (green line), osmotic (blue line), elastic (pink line), hydrophobic (purple line), and total (red line) interaction potentials of *OA-C16@CeO₂ 200* **(A)**, *OA-C18@CeO₂ 200* **(B)**, *OA-C16@CeO₂ 250* **(C)**, and *OA-C18@CeO₂ 250* **(D)**

Table S6. Parameters used to calculate interaction potentials

Sample	ρ / g mL^{-1}	MW / g mol^{-1}	γ x 10^{-3}/ mN m^{-1}	v_1 x 10^{-3} / mL mol^{-1}	L / nm	r / nm	A x 10^{-21} / nm	χ	ϕ
OA-C16@CeO₂ 200	0.940	241.5	3.07	2.97	2.2	4.4	-3.9	7.2	0.8
OA-C16@CeO₂ 200	0.813	267.5	3.14	3.10	2.5	4.2	-4.4	12.7	0.8
OA-C16@CeO₂ 250	0.940	241.5	3.07	2.97	2.2	2.9	-3.9	7.2	0.8
OA-C18@CeO₂ 250	0.813	267.5	3.14	3.10	2.5	2.5	-4.4	12.7	0.8

OA-amine@CeO_2 NPs: SANS data

Table S7. Parameters obtained by the fitting of SANS data of *OA-C18@CeO_2 250* sample

Sample	Core Radius / Å	Distance between two NPs / Å	$\rho_{core}10^{-6}$ / Å^{-2}	$\rho_{shell}10^{-6}$ / Å^{-2}	x_{C18}	x_{OA}
OA-C18@CeO_2 250	22.5 ± 0.3	35 ± 2	4.36 ± 0.03	0.017 ± 0.001	0.5	0.5

OA-amine@CeO_2 NPs: Optical Properties

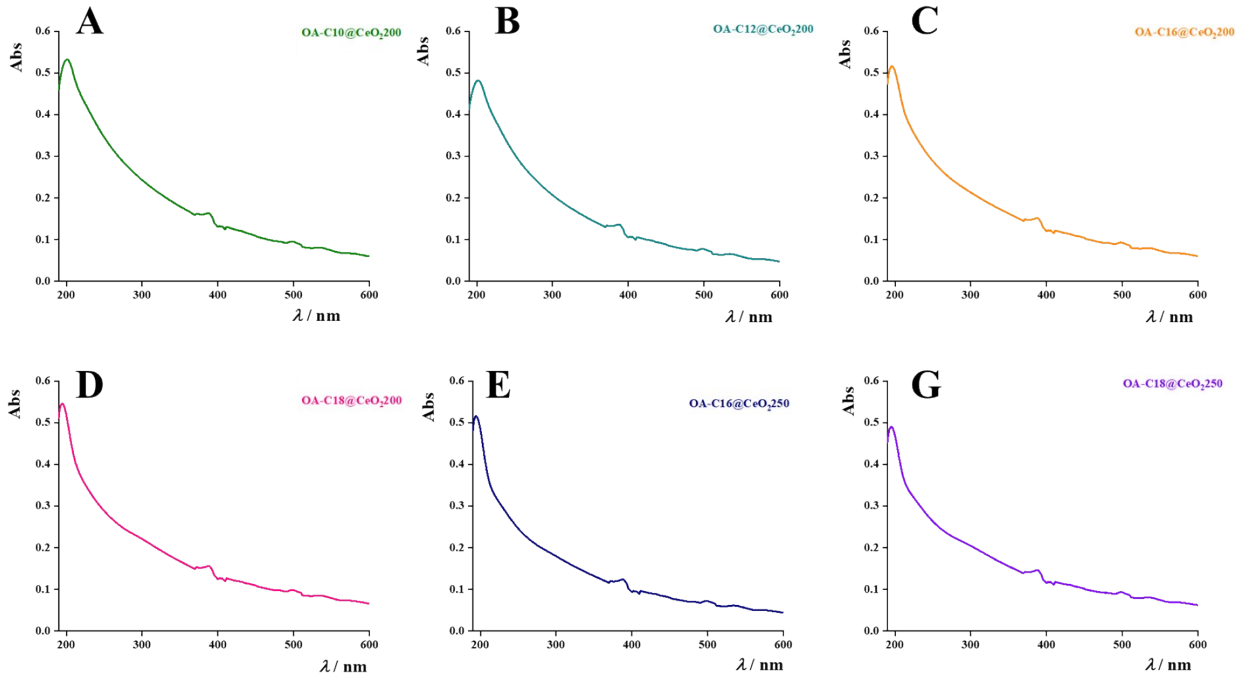

Figure S10. UV-Vis spectra of *OA-C10@CeO_2 200* **(A)**, *OA-C12@CeO_2 200* **(B)**, *OA-C16@CeO_2 200* **(C)**, *OA-C18@CeO_2 200* **(D)**, *OA-C16@CeO_2 250* **(E)**, *OA-C18@CeO_2 250* **(G)**.

References

[1] N. Gallucci, G. Vitiello, R. Di Girolamo, P. Imbimbo, D. M. Monti, O. Tarallo, A. Vergara, I. Russo Krauss, L. Paduano, *Nanomaterials* **2021**, *11*, 542.

[2] N. Gallucci, M.-S. Appavou, N. Cowieson, G. D'Errico, R. Di Girolamo, S. Lettieri, F. Sica, G. Vitiello, L. Paduano, *J Colloid Interface Sci* **2024**, *659*, 926.

[3] A. Rahdar, H. Beyzaei, F. Askari, G. Z. Kyzas, *Appl. Phys. A* **2020**, *126*, 324.

[4] D. Prieur, W. Bonani, K. Popa, O. Walter, K. W. Kriegsman, M. H. Engelhard, X. Guo, R. Eloirdi, T. Gouder, A. Beck, T. Vitova, A. C. Scheinost, K. Kvashnina, P. Martin, *Inorg. Chem.* **2020**, *59*, 5760.

[5] T. Mokkelbost, I. Kaus, T. Grande, M.-A. Einarsrud, *Chem. Mater.* **2004**, *16*, 5489.

[6] K. Liu, B. Yao, Y. Li, Z. Ding, H. Sun, Y. Jiang, G. Wang, D. Pan, *Journal of Materials Chemistry C* **2017**, *5*, 3035.

[7] A. Cangiano, N. Gallucci, A. Giarra, J. Ali, L. Chiappisi, N. P. Cowieson, L. Paduano, *Nanoscale* **2025**, *17*, 15829.

[8] M. Seyhan, W. Kucharczyk, U. E. Yarar, K. Rickard, D. Rende, N. Baysal, S. Bucak, R. Ozisik, *Nanotechnol Sci Appl* **2017**, *10*, 69.

[9] B. V. Tawade, M. Singh, I. E. Apata, J. Veerasamy, N. Pradhan, A. Karim, J. F. Douglas, D. Raghavan, *JACS Au* **2023**, *3*, 1365.
[10] B. Pansu, C. Goldmann, D. Constantin, M. Impéror-Clerc, J.-F. Sadoc, *Soft Matter* **2021**, *17*, 6461.